



Modelling eddy currents on a ferromagnetic plate: field in the conductor and magnetic permeability as a function of the frequency

Javier O Fava^{1,2}, Fernando D Carabedo¹, Marta C Ruch¹ and Marcelo Gutierrez²
1 Comisión Nacional de Energía Atómica, Argentina, fava@cnea.gov.ar
2 Facultad Regional Haedo, UTN, Argentina

Abstract

As a contribution to the design and construction of coils and sensors for the eddy current inspection of planar ferromagnetic components, results are presented from the modelling of a pancake coil on different ferromagnetic plates. This contribution is a solution to the well known problem of a cylindrical coil fed with a sinusoidal current of frequency f . The plate on which the coil lies has a thickness d , is infinite in the directions perpendicular to the coil axis, and has an electrical conductivity σ and a relative magnetic permeability μ_r .

Different ferromagnetic materials were selected for the research. The procedure is as follows: for each particular case, the electrical conductivity was first measured using van der Pauw's method. Then, given the geometry of the coils and the thickness and electrical conductivity of the plates, an inverse eddy current technique was applied, in order to determine the magnetic permeability at different ranges of the test frequency. This technique consists on a fitting of the impedance measurements using a least squares algorithm. The fitting function is calculated with the model and the parameter to be adjusted is the relative permeability. Thus effective values of the relative permeability are obtained, which may be interpreted as the valid parameters to be considered in an eddy current test.

1. Introduction

In the modelling of eddy current tests (ET) of ferromagnetic materials, the properties normally considered in the equations are the electrical conductivity and the relationship between the magnetic induction and the magnetic field $\mathbf{B} = \mathbf{B}(\mathbf{H})$. In these tests, the magnetic fields applied are so low that a lineal relationship between \mathbf{B} and \mathbf{H} can be assumed, the proportionality factor being the magnetic permeability μ , a tensor (which might be complex) depending on the position within the material and the test frequency (1). Assuming μ to be isotropic, locally constant and independent of frequency, then $\mathbf{B} = \mu \cdot \mathbf{H}$, and the impedance change of a coil on a planar metallic substrate can be calculated with models which have been simplified using these assumptions, such as that described in (2). However discrepancies between experiments on ferromagnetic materials, (3) and (4), and the predictions of those simple models suggest that some of these simplifications must be reconsidered. A study of the variation of μ in a large frequency interval (5) suggests that models in which μ is considered to be independent from frequency are not adequate for the modelling of ET in these conditions.



In our laboratory, theoretical solutions for coil impedance have been previously deduced, in which test parameters (frequency, lift-off, geometry of coil and test piece) and material parameters (magnetic permeability and electrical conductivity) are considered. These models can be applied to material characterization, by using them to solve the inverse problem for material parameters, (5), (6) and (7).

In what follows, theoretical and experimental evaluation of the relative permeability, μ_r , of a set of ferromagnetic steels is presented. Given the conductivity values and the model, the calculations leading to μ_r as a function of frequency are analyzed. Then, the fields within the test piece and outside it are modelled at a particular test frequency.

2. Materials

2.1 Samples and coils

Four planar samples of ferromagnetic steels were studied (d = sample thickness):

- a) SAE 1010 (75 x 75 x $d=6.5$) mm³.
- b) SAE 1022 (225 x 80 x $d=6.5$) mm³.
- c) AISI 347 (65 x 30 x $d=2.3$) mm³ (cold rolled austenitic stainless steel, containing 87 wt% ferromagnetic α' martensite).
- d) SAE 1566 (0.63%C) (70 x 30 x $d=3.4$) mm³, taken from a piece of railway track.

The electrical conductivities of these samples were measured by van der Pauw's method as described in (6). Sample identification and conductivity are presented in table 1.

Table 1. Conductivity of studied samples.

Sample	SAE 1010 M1010	SAE 1022 M1022	AISI 347 M347	SAE 1566 M1566
Conductivity (MS/m)	3.83±0.06	5.76±0.09	1.05±0.02	3.68±0.06

Three cylindrical coils having the parameters in table 2 were used (refer to figure 1).

Table 2. Coils.

Coil	r_1 (mm)	r_2 (mm)	$z_2 - z_1$ (mm)	N
1	1.0±0.1	2.95±0.06	2.5±0.1	387
2	4.0±0.1	4.5±0.1	15.0±0.1	400
3	4.0±0.1	5.0±0.1	15.0±0.1	800

3. Determination of relative permeabilities (μ_r)

3.1 Theoretical model for μ_r

A particular case of the formulas deduced in section 3.3, page 64 of (2) was used to calculate the theoretical impedance change ΔZ^T of a cylindrical coil on a conductive plate. The problem solved is shown in figure 1.

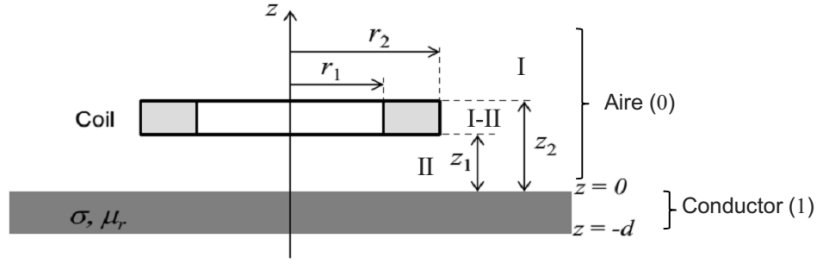


Figure 1: Electromagnetic problem.

$$\Delta Z^T = Z^T - Z_0 = \frac{j\pi\omega\mu_0 N^2}{(r_2 - r_1)^2 (z_2 - z_1)^2} \int_0^\infty \frac{\Gamma^2(\kappa r_1, \kappa r_2)}{\kappa^6} (e^{-\kappa z_1} - e^{-\kappa z_2})^2 \cdot \frac{(\lambda^2 - \kappa^2 \mu_r^2)(e^{-2\lambda d} - 1)}{(\lambda + \kappa \mu_r)^2 - e^{-2\lambda d} (\lambda - \kappa \mu_r)^2} d\kappa \quad (1)$$

Z^T is coil impedance on the conductor, Z_0 is coil impedance in air, z_1 is lift-off, N is number of turns in the coil, $\lambda = \sqrt{\kappa^2 + k^2}$ ($k^2 = j\omega\mu_r\mu_0\sigma$); for the other functions and parameters en equation (1), see (2). As usual in ET, impedance is normalized to the inductive reactance of the coil in air: $\Delta Z^{T,N} = \Delta Z^T / \omega L_0$.

The relative magnetic permeability was calculated with the inverse ET technique described in (5), (7) and (8), which consists in making a non-linear fit of the experimental normalized impedance change of the coil ($\Delta Z^{E,N}$) with the corresponding theoretical variable ($\Delta Z^{T,N}$, equation (1)).

The function to be minimized, χ^2 , was constructed with the imaginary parts of the normalized impedance changes: $\text{Im}(\Delta Z^{T,N})$ and $\text{Im}(\Delta Z^{E,N})$: $\chi^2(\mu_r) = \sum_{k=1}^N \left\{ \left[\text{Im}(\Delta Z^{E,N}(k)) - \text{Im}(\Delta Z^{T,N}(k)) \right]^2 / (W_k)^2 \right\}$. The measurements of $\Delta Z^{E,N}$ were made at frequencies f_k with $k=1, 2, \dots, N$.

3.2 Procedure for the measurement of relative permeability

3.2.1 Coil and impedance measurement

Coil number 1 in table 2 was used for permeability evaluation. Coil impedances were measured with an impedance analyzer Solartron SI 1260, in the frequency ranges:

a) 1 kHz to 1 MHz, with a logarithmic scan of 10 points per decade; hence $N=31$, with $f_1=1$ kHz and $f_N=1$ MHz. A μ_r value was calculated for the whole range and then particular μ_r for each decade.

b) The second decade of scan a) with a 1 kHz increment in frequency, and the μ_r values were calculated for the 9 sub-intervals: 10-20 kHz, ..., 90 kHz-100 kHz.

3.2.2 Adjustment of the relative magnetic permeability

The permeability of the samples was determined using the theoretical model in 3.1 and the conductivities in table 1, at the frequency intervals established in 3.2.1. Thus the only unknown parameter to be adjusted was the relative permeability. A Montecarlo type analysis was used to evaluate the uncertainty of the relative magnetic permeability, see (8) for details.

4. Magnetic fields

The magnetic field was calculated around the coils which are used in an inspection device under construction in the laboratory (9): coils 2 and 3 in table 2. Nominal lift-off of these coils was $z_1 = (0.40 \pm 0.05)$ mm. A model of a semi-infinite conductor was used, such as that in figure 1, but with $d \rightarrow -\infty$. Equations for the fields in the denoted region of figure 1 (Aire (0) and Conductor (1) with $d \rightarrow -\infty$) were taken from chapter 3 in reference (2). These solutions were programmed in MatlabTM.

5. Results

5.1 Studies of magnetic permeability as a function of frequency

Because parameters calculated with a model like ours are normally called “effective parameters”, the calculated permeabilities will be identified here as “effective relative permeabilities” $\mu_{r, \text{effective}}$. Table 3 presents the calculated magnetic permeabilities of the four steels in the full frequency range (1 kHz-1 MHz) and in each of the three decades in which this range can be divided. Figure 2 illustrates the fit between experimental results and the theoretical model for the full frequency range in the cases of M1022 and M347 samples.

Table 3. $\mu_{r, \text{effective}}$ in the full frequency range and in the 3 decades of that range.

Frequency range	$\mu_{r, \text{effective}}$			
	M1010	M1022	M347	M1566
1 kHz – 1 MHz	121±3	95±2	54±1	38±1
1 kHz – 10 kHz	181±5	116±3	60±2	38±1
10 kHz – 100 kHz	120±3	101±3	57±1	39±1
100 kHz – 1 MHz	67±2	72±2	49±1	38±1

As the test frequency increases, a decrease of $\mu_{r, \text{effective}}$ is observed for the studied samples, except for M1566, for $\mu_{r, \text{effective}}$ is nearly constant. These results indicate the interaction of these ferromagnetic materials with the electromagnetic field produced by the coil. Figure 3 illustrates the fit between experimental and theoretical results of samples M1010 y M1566, separated in decades.

The central decade in figure 3 and table 3 (10 kHz - 100 kHz) was further divided in nine subintervals, and the $\mu_{r, \text{effective}}$ were recalculated (case **b**) in 3.2). These results are presented in table 4 and illustrated in figure 4 for samples M1022 and M347. As before, a decrease of $\mu_{r, \text{effective}}$ with the test frequency is observed, except for sample M1566.

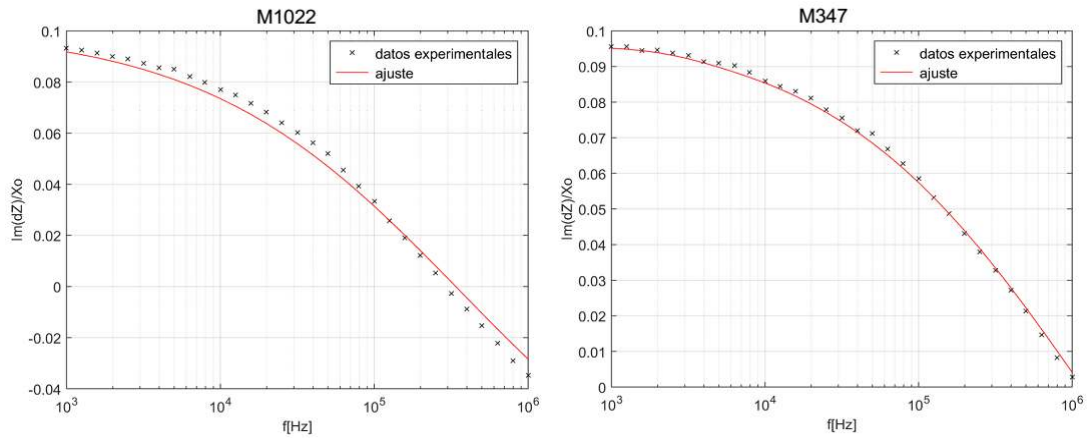


Figure 2. Experimental and adjusted data. Full frequency range: 1 kHz – 1 MHz. Samples M1022 and M347. Table 3

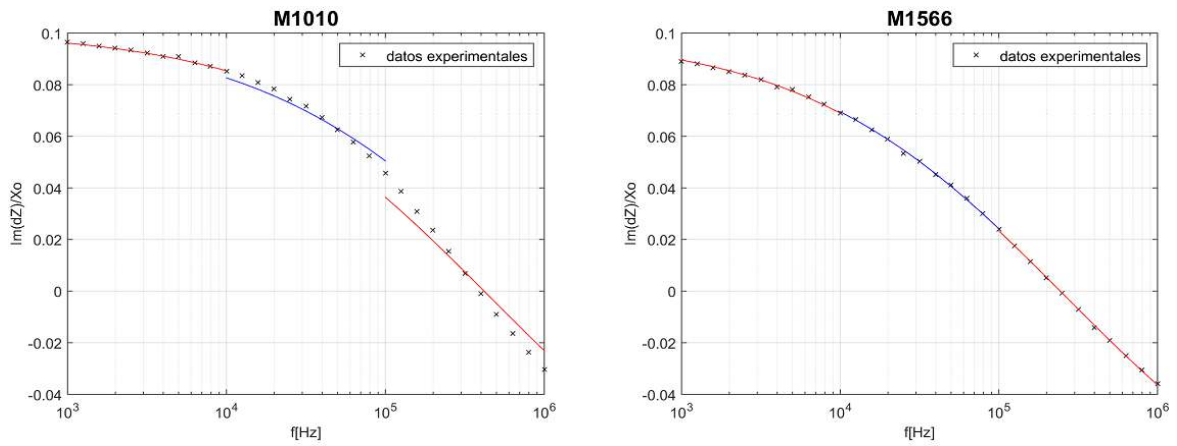


Figure 3. Experimental and adjusted data per decade: 1 kHz – 10 kHz, 10 kHz – 100 kHz and 100 kHz – 1 MHz. M1010 and M1566. Table 3.

Table 4. $\mu_{r, \text{effective}}$ for each subinterval in the 10 kHz – 100 kHz decade.

Frequency range	$\mu_{r, \text{effective}}$			
	M1010	M1022	M347	M1566
10 kHz – 20 kHz	168±4	112±3	59±1	39±1
20 kHz – 30 kHz	154±4	108±3	57±1	39±1
30 kHz – 40 kHz	142±4	103±3	55±1	39±1
40 kHz – 50 kHz	133±3	99±2	55±1	39±1
50 kHz – 60 kHz	124±3	95±2	54±1	39±1
60 kHz – 70 kHz	117±3	93±2	54±1	38±1
70 kHz – 80 kHz	113±3	91±2	53±1	38±1
80 kHz – 90 kHz	108±3	89±2	53±1	38±1
90 kHz – 100 kHz	104±3	87±2	52±1	38±1

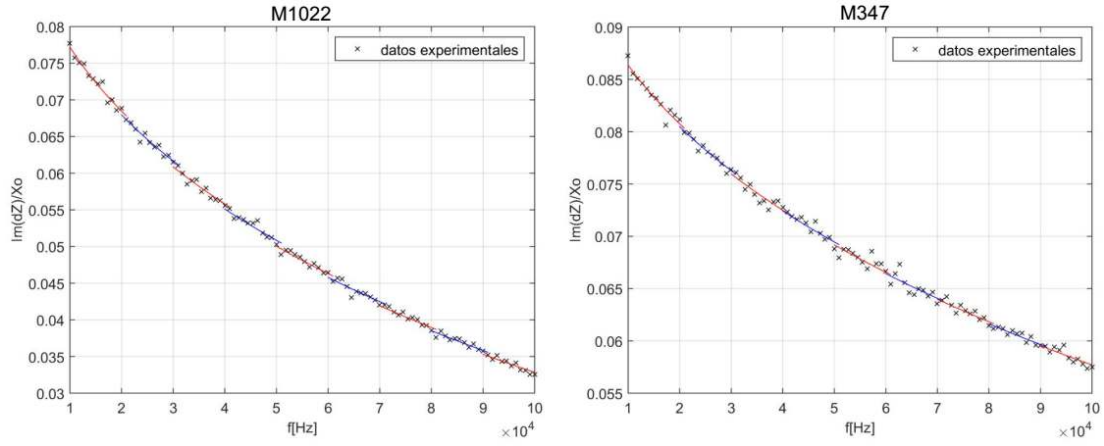


Figure 4. Experimental and adjusted data, table 4. M1022 and M347.

5.2 Modelling of the magnetic field

The figures in this section present some examples of the distribution of the calculated magnetic field \mathbf{B} in the regions surrounding the coil. The modulus of \mathbf{B} (normalized with respect to its maximum value) is represented in the r - z plane, with z the vertical axis and the conductive material in the range $z < 0$.

As mentioned in Section 4, one of the objectives of this work is to contribute to the design of the coils used in the device and experiments described in (9). Coils 2 and 3 in table 2 are used in that reference, together with two calibration pieces: a planar one made of carbon steel (sample M1010) with grooves and a portion of railroad track (sample M1566) with cracks. Good experimental results were obtained in (9) for frequencies in the range 25 to 40 kHz; results of the modelling of \mathbf{B} at 35 kHz are shown here, together with results at 5 kHz, in order to highlight the effect of the ferromagnetic field within the conductor.

Figure 5 shows the modulus of \mathbf{B} in coil 3 on sample M1566, at 5 kHz. Conductivity and permeability for the model are taken from tables 1 and 3 (row 2) respectively.

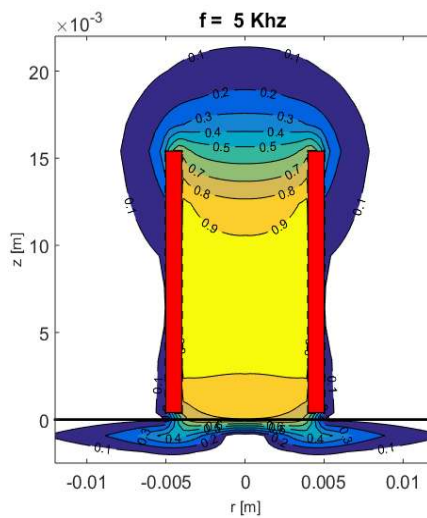


Figure 5. Modulus of \mathbf{B} , coil 3, at 5 kHz, $\mu_{r, \text{effective}} = 38$ (sample M1566, first decade, table 3, row 2)

In figure 6 comparisons are made of the results for coil 2 (N=400, figure (a)) and coil 3 (N=800, figure (b)), for material of sample M1010, at test frequencies: 5 kHz and 35 kHz. As before, electrical conductivity is taken from table 1 and relative magnetic permeability from row 2 of table 3 for figure 6 (a) (f = 5 kHz) $\mu_{r, \text{effective}} = 181$ and from row 3 of table 4 for figure 6 (b) (f = 35 kHz) $\mu_{r, \text{effective}} = 142$. In the simulations at 5 kHz the field expands within the ferromagnetic conductor. As the test frequency increases, field attenuation within the conductor is more significant and, at 35 kHz, the field is fully concentrated under the coil. Similar results were obtained for the other materials.

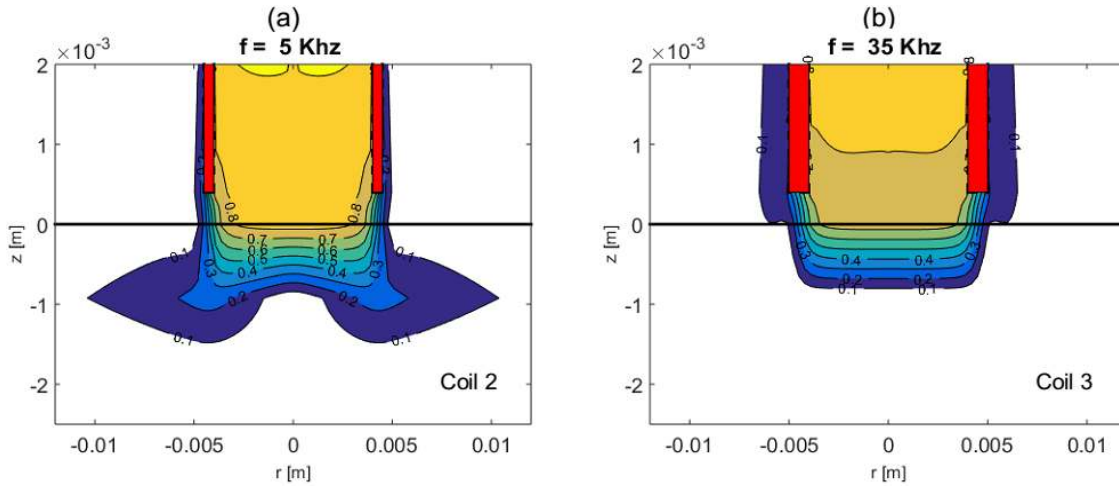


Figure 6. Modulus of B. Comparison of coils 2 and 3, sample M1010. Region near the conductor.

6. Conclusions

An inverse ET technique was used to evaluate the permeabilities of samples of ferromagnetic steels. It is concluded that μ_r as an ET effective parameter depends on test frequency. Although this had already been established in (5), in the present work the conductivities of the tested materials were better known, and more points in the different intervals were measured. The concept “effective parameter” refers to a value calculated with a method such as that presented in 3.1. This means that the interaction of the electromagnetic wave with the material is not simply determined by the values of the parameters used in the standard skin depth formula: $\delta = \sqrt{2/\omega\mu\sigma}$; but in the case of permeability, the behaviour of the material at different test frequencies must be evaluated by comparison between experimental results and the output of a theoretical model.

Ranges of frequencies could be established by inspection of the values of μ_r in tables 3 and 4, for which the description provided by the theoretical model is adequate for EC tests of the materials in this work. In particular μ_r of material M1566 is almost constant in the frequency range used here; this is not the case for the other samples: M1010 and M1022 present the largest variation, while μ_r of M347 decreases slightly with an increase in frequency. It might be assumed that the behaviour is determined by the chemical composition and microstructure of the material. Hence a study of these conditions of the four alloys should be undertaken in the near future.

Because in the models of \mathbf{B} presented here, adjusted permeability values specifically determined for each particular frequency interval, are used, it can be said that these models are more exact than those based on general tabulated values of μ_r .

In the setup studied here, it was possible to observe the influence of the ferromagnetic material on the distribution of \mathbf{B} at low frequency, and the concentration of the field very close to the coil at frequencies higher than 20 kHz. \mathbf{B} falls to 10% of its maximum value at 1.5 mm from the coil (or even closer to it). These results help evaluate the influence of edge effect, the closeness to a crack or to other coils. It must be born in mind that in this modelling of coil/material interaction, no discussion is made of the electric or electronic factors which define the performance of an EC equipment.

Acknowledgements

To Esteban Bisignano, from CAC-CNEA, for the machining of samples.

References

1. J Rose, E Uzal, and J Moulder, "Magnetic Permeability and Eddy-Current Measurements", Rev. Progress in Quantitative NDE, Vol 14, pp 315-322, 1995.
2. T Theodoulidis and E Kriezis, "Eddy Current Canonical Problems (with Applications to Nondestructive Evaluation)", Forsyth: Tech Science Press, 2006.
3. J Rose, C-C Tai and J Moulder, "Scaling Relation for the Inductance of a Coil on a Ferromagnetic Half-Space", J. App. Phys., Vol 82, No 9, pp 4604-4610, 1997.
4. J Moulder, C-C Tai, B Larson and J Rose, "Inductance of a Coil on a Thick Ferromagnetic Metal Plate", IEEE Trans. Mag., Vol 34, No 2, pp 505-514, 1998.
5. G Cosarinsky, J Fava, M Ruch, M Georgetti and A. Bonomi, "Determinación de permeabilidades magnéticas en mediciones de corrientes inducidas", IX CORENDE (Congreso Regional de Ensayos no Destructivos y Estructurales), Mar del Plata, Buenos Aires, Argentina, 2-4 octubre 2013.
6. G Cosarinsky, J Fava, M Ruch y Adrián Bonomi, "Material Characterization by Electrical Conductivity Assessment Using Impedance Analysis", Proc. Mat. Science, Vol 9, pp 156-162, 2015.
7. J Fava, C Spinosa, M Ruch, F Carabedo, M Landau, G Cosarinsky, A Savin, R Steigmann y M Craus, "Characterization of the Reverse Martensitic Transformation in Cold-Rolled Austenitic 316 Stainless Steel", 16° Congreso Internacional de Metalurgia y Materiales SAM-CONAMET/IBEROMAT; Córdoba, Argentina, 22-25 noviembre, 2016.
8. J Fava, F Carabedo, y C Spinosa, "Evaluación del contenido de martensita en aceros inoxidable austeníticos laminados en frío", Technical Report: IN-13-E-151-IM/16, Comisión Nacional de Energía Atómica, 2016.
9. M Gutiérrez, J Fava, T Di Fiore, M Ruch, R Romero, y Juan Vorobioff, "Development of a differential test device for eddy current rail inspection", abstract accepted for the 12th European Conference on Non-Destructive Testing (12th ECNDT) Conference, Gothenburg, Sweden, June 11-15 2018.